



PRMT5 links lipid metabolism to contractile function of skeletal muscles

Kun Ho Kim¹ , Zhihao Jia¹, Madigan Snyder^{1,2}, Jingjuan Chen¹, Jiamin Qiu¹, Stephanie N Oprescu^{1,2}, Xiyue Chen¹, Sabriya A Syed³, Feng Yue¹, Bruno T Roseguini⁴, Anthony N Imbalzano³, Changdeng Hu^{5,6,†} & Shihuan Kuang^{1,6,*} 

Abstract

Skeletal muscle plays a key role in systemic energy homeostasis besides its contractile function, but what links these functions is poorly defined. Protein Arginine Methyl Transferase 5 (PRMT5) is a well-known oncoprotein but also expressed in healthy tissues with unclear physiological functions. As adult muscles express high levels of *Prmt5*, we generated skeletal muscle-specific *Prmt5* knockout (*Prmt5^{MKO}*) mice. We observe reduced muscle mass, oxidative capacity, force production, and exercise performance in *Prmt5^{MKO}* mice. The motor deficiency is associated with scarce lipid droplets in myofibers due to defects in lipid biosynthesis and accelerated degradation. Specifically, PRMT5 deletion reduces dimethylation and stability of Sterol Regulatory Element-Binding Transcription Factor 1a (SREBP1a), a master regulator of *de novo* lipogenesis. Moreover, *Prmt5^{MKO}* impairs the repressive H4R3 symmetric dimethylation at the *Pnpla2* promoter, elevating the level of its encoded protein ATGL, the rate-limiting enzyme catalyzing lipolysis. Accordingly, skeletal muscle-specific double knockout of *Pnpla2* and *Prmt5* normalizes muscle mass and function. Together, our findings delineate a physiological function of PRMT5 in linking lipid metabolism to contractile function of myofibers.

Keywords lipid droplet; lipolysis; myofiber; posttranslational modification; protein arginine methyltransferase

Subject Category Metabolism

DOI 10.15252/embr.202357306 | Received 6 April 2023 | Revised 30 May 2023 |

Accepted 5 June 2023 | Published online 19 June 2023

EMBO Reports (2023) 24: e57306

Introduction

Skeletal muscles cells (also called myofibers) are multinucleated contractile units that empower body movements and mobility. The skeletal muscle also plays a key role in systemic energy homeostasis through glucose disposal and fatty acid oxidation (FAO) (Chargé & Rudnicki, 2004; Bassel-Duby & Olson, 2006). A progressive decline in skeletal muscle mass and function not only impairs exercise capacity but also increases the risks of metabolic disorders associated with cellular oxidative stress, mitochondrial dysfunction, and insulin resistance (Kim & Kim, 2020). Muscle atrophy, one of the most destructive features of muscular dysfunction, results from protein degradation that reduces muscle mass. Additionally, an oxidative-to-glycolytic conversion of myofibers renders them more prone to protein degradation, leading to nutrient-related atrophy (Sandri, 2008; Bonaldo & Sandri, 2013; Wang & Pessin, 2013).

Intramyocellular lipid (IMCL) is a crucial energy source for FAO, serves as an important building block for cellular and organelle membranes, and generates bioactive metabolites that mediate various signaling pathways (Consitt *et al*, 2009; Morales *et al*, 2017). Intramyocellular lipid is typically stored in lipid droplets (LDs), cytoplasmic organelles that store and release lipids such as triglycerides (TAG). Dynamics of LDs are linked to a myriad of physiological and pathological processes (Welte & Gould, 2017; Olzmann & Carvalho, 2019; Seibert *et al*, 2020). Lipid droplet biogenesis is mediated by TAG-synthesizing enzymes under the control of transcriptional factors such as SREBP1 (Hagen *et al*, 2010). Lipid droplet turnover is mediated by lipolysis that liberates fatty acids (FAs) from TAG for oxidation as a source of energy. The first and rate-limiting step in lipolysis is catalyzed by adipose triglyceride lipase (ATGL, encoded by *Pnpla2* gene) to hydrolyze TAG to generate a free FAs and DAG (diacylglycerols; Badin *et al*, 2012; Watt & Hoy, 2012). Dysfunctional ATGL-mediated lipolysis in myofibers reduces the availability of

¹ Department of Animal Sciences, Purdue University, West Lafayette, IN, USA

² Department of Biological Sciences, Purdue University, West Lafayette, IN, USA

³ Department of Biochemistry and Molecular Pharmacology, University of Massachusetts Medical School, Worcester, MA, USA

⁴ Department of Health and Kinesiology, Purdue University, West Lafayette, IN, USA

⁵ Department of Medicinal Chemistry and Molecular Pharmacology, Purdue University, West Lafayette, IN, USA

⁶ Center for Cancer Research, Purdue University, West Lafayette, IN, USA

*Corresponding author. Tel: +1 765 4948283; E-mail: skuang@purdue.edu

[†]Deceased.

FAs for energy conversion and impairs muscle function (Kim et al, 2008; Badin et al, 2012; Onal et al, 2017; Debashree et al, 2018). Conversely, increased ATGL activity is associated with muscle wasting in cancer cachexia (Das et al, 2011). Despite the known function of ATGL in skeletal muscle and muscle satellite cells (Sitnick et al, 2013; Dubé et al, 2015; Meex et al, 2015; Yue et al, 2022), what regulates lipid metabolism in the skeletal muscle is poorly understood.

Protein methylation, a common posttranslational modification (PTM) that results in the addition of methyl groups to lysine or arginine residues, has been involved in protein functional modulation, affecting signaling transduction and gene transcription (Lee et al, 2005; Ng et al, 2009; Moore et al, 2013; Murn & Shi, 2017). Protein arginine methyltransferases (PRMTs), composed of nine paralogs, can catalyze methylation of a broad range of substrates, including histone proteins (Lee et al, 2005; Guccione & Richard, 2019). Histone arginine methylation is associated with dynamic gene regulation, as chromatin structure remodeling either leads to activation or repression of targeted genes (Litt et al, 2009; di Lorenzo & Bedford, 2011). For example, symmetric dimethylation of histone 4 arginine 3 (H4R3Me2s) associated with several genes has been reported to underly pathogenesis of cancer (Ancelin et al, 2006; Wang et al, 2008; Deng et al, 2017). Recent studies have reported that PRMT1, PRMT4, PRMT7 regulates a variety of biological processes in the skeletal muscle (Wang et al, 2012; Jeong et al, 2016, 2020; Choi et al, 2019). Previous studies also reported that PRMT5 is indispensable for the proliferation and differentiation of myogenic progenitors and skeletal muscle regeneration (Dacwag et al, 2007; Zhang et al, 2015).

In this study, we characterized the function of PRMT5 in myofibers through *Myl1^{cre}*-driven knockout of *Prmt5* (*Prmt5^{MKO}*) in mice. The *Prmt5^{MKO}* mice exhibited reduced muscle mass and body weight along with impaired contractile function and motor performance. The *Prmt5^{MKO}* mice also contained an increased proportion of glycolytic myofibers and reduced proportion of oxidative myofibers. Molecular analysis revealed that PRMT5 promotes methylation of mSREBP1a (mature SREBP1a) in skeletal muscles to upregulate lipogenic genes. Moreover, PRMT5 epigenetically represses the transcription of *Pnpla2* gene (encoding ATGL) via H4R3Me2s. Consistently, ablation of *Pnpla2* gene in *Prmt5^{MKO}* mice (muscle-specific *Prmt5/Pnpla2* double KO) fully rescued the contractile phenotypes of the *Prmt5^{MKO}* mice. Collectively, these data establish a novel function of PRMT5 as a regulator of lipid metabolism in myofibers that subsequently affect muscle development and contractile function.

Results

Myofiber-specific *Prmt5* KO reduces muscle mass in adult mice

We first examined *Prmt5* gene expression in postnatal hindlimb muscles. Among the seven PRMTs, mRNA level of *Prmt5* was significantly higher than other isoforms (Fig EV1A). In addition, *Prmt5* mRNA level in the skeletal muscle was the highest among various human tissues, though every tissue expressed *Prmt5* abundantly (Fig EV1B; Uhlén et al, 2015). We also assessed the expression of *Prmt5* during muscle satellite cell differentiation, using publicly available Tabula Muris and single-cell RNA sequencing (scRNA-seq) data (Yue et al, 2022), and found that only 8% of satellite cells have detectable levels of *Prmt5*, while the remainder 92% have undetectable level of *Prmt5* (Appendix Fig S1). Violin plots clearly highlighted that *Prmt5* expression is dramatically increased during differentiation correlated with *MyoG* expression (Fig EV1C). We therefore hypothesized that PRMT5 plays a key role in the postdifferentiation skeletal muscle. To test this hypothesis, we generated skeletal muscle specific *Prmt5* knockout mice (abbreviated as *Prmt5^{MKO}*) by crossing *Prmt5^{lox/lox}* mice with *Myl1^{cre}* knockin mice expressing Cre recombinase driven by the endogenous *myosin light chain 1* (*Myl1*) gene. In this mouse model, the frameshift deletion of exon 7 causes a premature stop codon, resulting in a truncated protein of only 220 amino acids excluding all the key functional domain (Fig 1A). A specific reduction of *Prmt5* in skeletal muscle was validated in *Prmt5^{MKO}* mice in comparison with WT mice (Fig EV1D).

The *Prmt5^{MKO}* mice were born normally but appeared leaner than their WT littermates starting at 6-week-old, despite similar food intake (Fig 1B–D). EcoMRI body composition measurements revealed that the reduced body weights in the 2-month-old KO mice is associated with significant reduction in lean mass (muscle) but not in fat mass (Fig 1E). Consistently, the 2-month-old *Prmt5^{MKO}* mice had smaller skeletal muscles, including Sol (Soleus), EDL (Extensor digitorum longus), TA (Tibialis anterior), GAS (Gastrocnemius), and QU (Quadriceps) muscles, than WT counterparts (Fig 1F and G). In contrast, fat masses of various depots including iWAT (Inguinal white adipose tissue) and BAT (Brown adipose tissue) were similar between the WT and KO mice (Fig EV1E). We also measured myofiber size based on cross-sectional area (CSA) in TA muscle sections after H&E staining and immunofluorescence staining of dystrophin (Fig 1H and I). A leftward shift in the distribution of myofiber sizes was observed in 2-month-old *Prmt5^{MKO}* mice (Fig 1J), and the average CSA of the TA muscle in *Prmt5^{MKO}* mice was significantly smaller than that of WT muscles (Fig 1K),

Figure 1. Muscle-specific knockout of PRMT5 (*Prmt5^{MKO}*) leads to muscle mass reduction.

- A Genetic targeting strategy showing skeletal muscle-specific deletion of *Prmt5* using the *Cre-LoxP* recombinase under the control of the *Myl1* promoter.
- B, C Representative images of 2-month-old mice (B) and growth curves (C) of WT ($n = 6$) and *Prmt5^{MKO}* mice ($n = 6$).
- D Food intake normalized to body weight in WT ($n = 4$) and *Prmt5^{MKO}* mice ($n = 3$).
- E Lean and fat mass in WT ($n = 4$) and *Prmt5^{MKO}* mice ($n = 4$) determined by EcoMRI body composition analyzer.
- F Photographs of skeletal muscles in 2-month-old WT and *Prmt5^{MKO}* mice.
- G The quantified weight of muscles (SOL, EDL, TA, GAS, QU) in 2-month-old WT ($n = 4$) and *Prmt5^{MKO}* mice ($n = 4$).
- H, I Representative H&E (H) and dystrophin immunofluorescence of images of TA muscle cross-sections in WT and *Prmt5^{MKO}* mice. Scale bar: 100 μm .
- J, K Distribution of myofiber size (J) and average myofiber cross-sectional area (CSA) (K) of WT ($n = 4$) and *Prmt5^{MKO}* TA muscles ($n = 4$).
- L The total number of myofibers in EDL and Soleus from WT ($n = 5$) and *Prmt5^{MKO}* mice ($n = 6$).

Data information: The data are presented as mean \pm SEM and *P*-values determined by two-tailed ANOVA unpaired *t*-test based on sample sizes (biological replicates) shown in (C–E, G, J, K, L) (**P* < 0.05, ***P* < 0.01, ****P* < 0.001, *****P* < 0.0001).

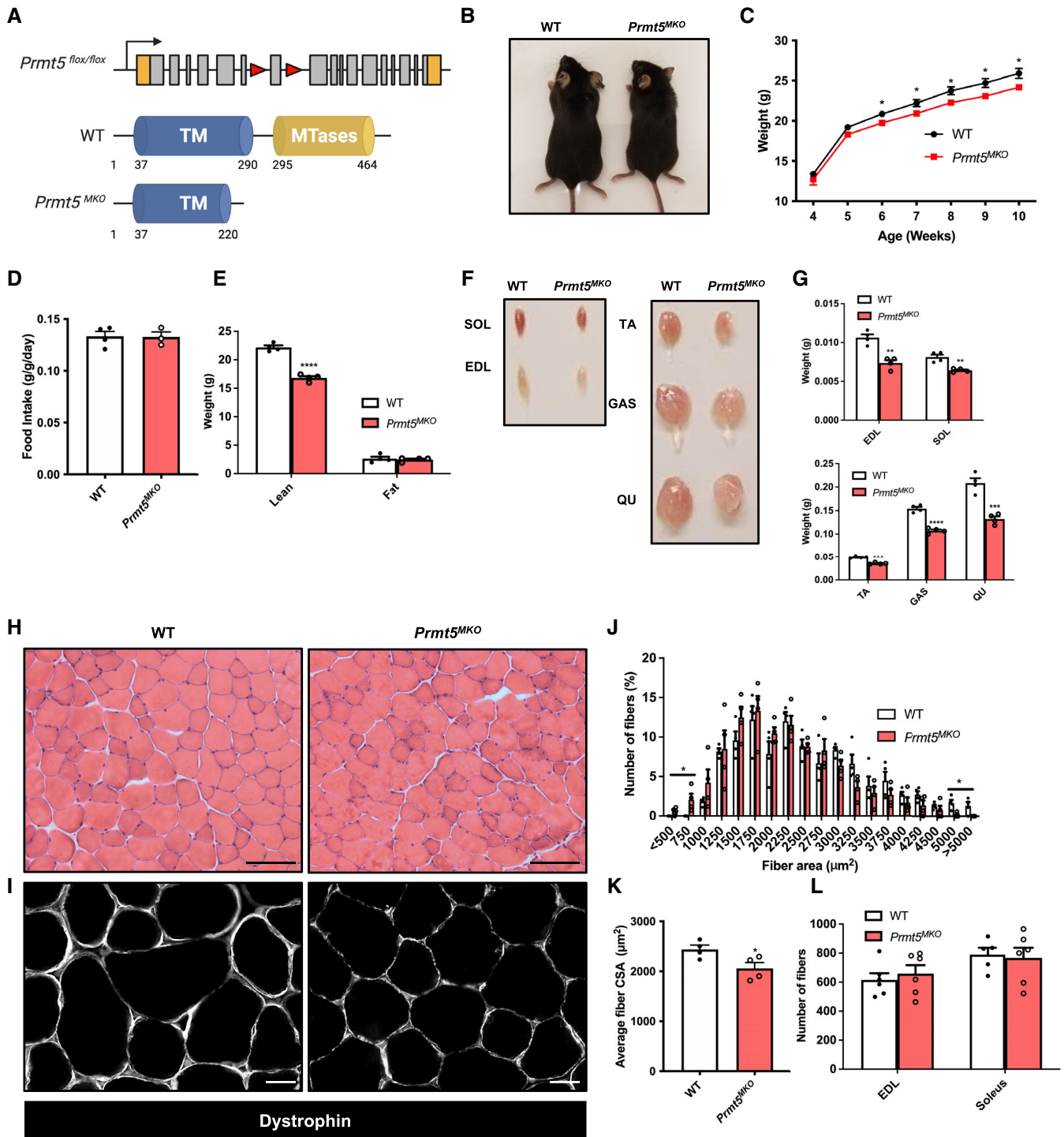


Figure 1.

but the total number of myofibers in the EDL and Soleus muscles was similar[#] between WT and *Prmt5*^{MKO} mice (Fig 1L).

To determine whether reduced myofiber size is due to protein degradation, we examined expression of Atrogin-1 and MuRF-1 (encoded by *Fbxo32* and *Trim63* gene respectively), markers for

muscle-specific E3 ubiquitin ligases involved in the breakdown of muscle proteins during muscle atrophy. The levels of Atrogin-1 and MuRF1 were similar between WT and KO muscle tissues (Fig EV1F). This suggests that alternative pathways contributed to muscle atrophy independent of the ubiquitin-proteasome system. We then

[#]Correction added on 3 August 2023, after first online publication: “similar” has been added to this sentence.

investigated early stages of postnatal muscle growth (before weaning) by measuring the average size and total number of myofibers in TA muscles at postnatal day (P) P7 and P21. The results showed no difference in myofiber size and number between WT and *Prmt5^{MKO}* mice (Fig EV2A–C). These results suggest that PRMT5 in myofiber does not affect muscle development and early growth.

To further determine whether muscle-specific loss of PRMT5 affect myofiber-associated Pax7⁺ satellite cells that are essential for nuclei accretion during muscle growth, we quantified the number of Pax7⁺ cells in muscle tissues and freshly isolated myofibers. A similar number of Pax7⁺ satellite cells was found in WT and *Prmt5^{MKO}* mice (Fig EV2D and E). We also assessed whether *Prmt5^{MKO}* affects regeneration of muscle tissue after cardiotoxin (CTX)-induced injury, but muscle histology and newly regenerated myofibers (marked by eMyHC) did not exhibit significant differences between WT and *Prmt5^{MKO}* mice (Fig EV2F and G). These results together suggest that *Prmt5^{MKO}* does not affect embryonic myogenesis, early growth, and postnatal muscle regeneration, but affect postnatal muscle maintenance.

Prmt5 KO impairs motor performance and muscle contractile function

We examined muscle functions based on several physiological measurements. The grip strength of *Prmt5^{MKO}* mice was significantly weaker than that of WT mice (Fig 2A). When mice were run on a treadmill, the *Prmt5^{MKO}* mice exhibited significantly lower maximum speed, running time, and running distance than did their littermate controls (Fig 2B–D). To explore whether the reduced grip strength and exercise performance of *Prmt5^{MKO}* mice was due to attenuated muscle contractile function, we assessed force generation capacity of the isolated fast-twitch EDL and slow-twitch Soleus muscles. Force development of the EDL and Soleus muscles was measured over a range of stimulation frequencies (Fig 2E and F). The maximum absolute force of the EDL and Soleus muscles was reduced by 40 and 22%, respectively, in the KO mice relative to WT animals (Fig 2E and F). A similar trend was observed in specific force, when absolute force was normalized to muscle CSA (Fig 2G

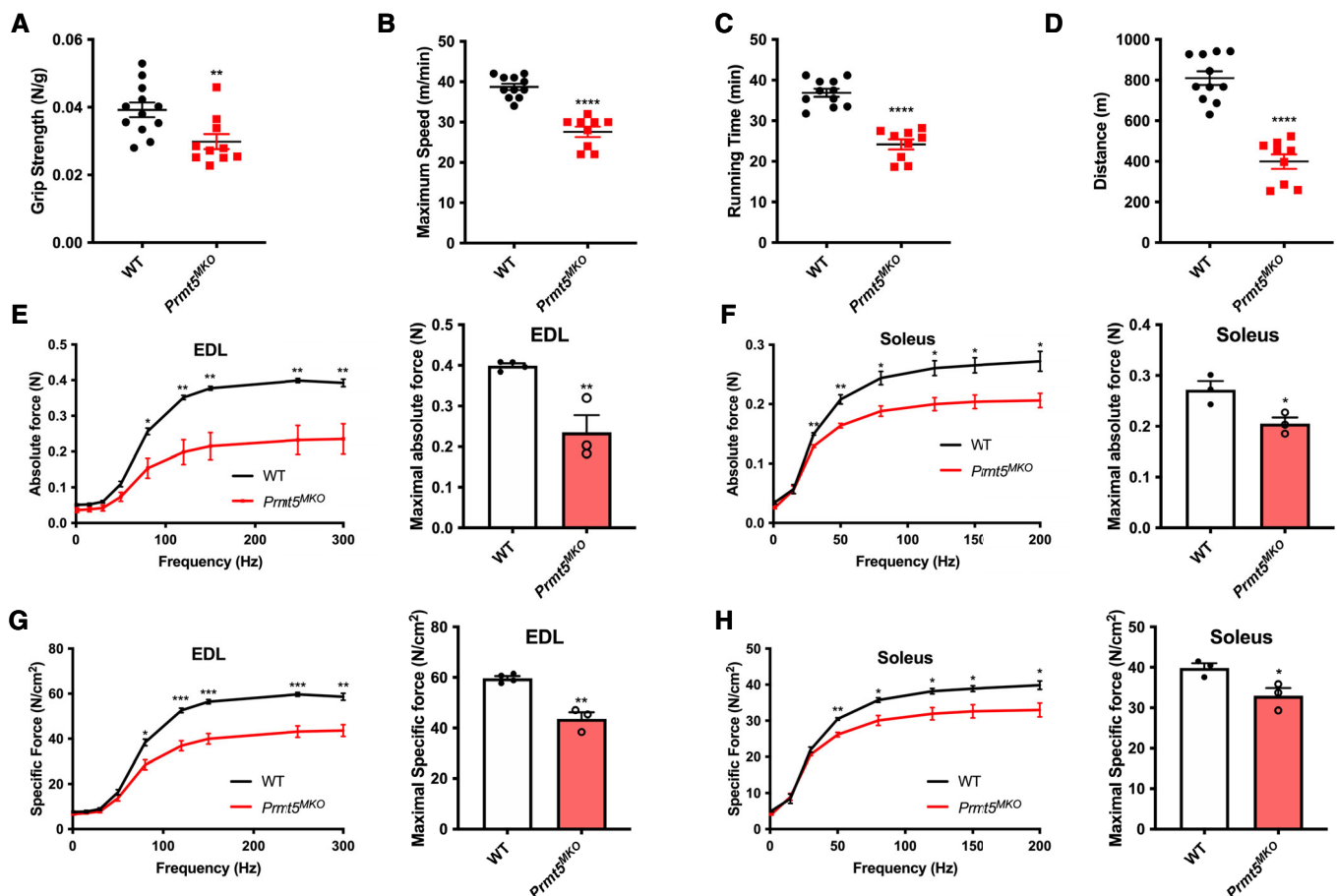


Figure 2. Reduced motor-performance and muscle contractile function in 2-month-old *Prmt5^{MKO}* mice.

A Grip strength tests of WT and *Prmt5^{MKO}* mice assessed by grip force normalized to body weight WT ($n = 12$) and *Prmt5^{MKO}* mice ($n = 10$).
 B–D Exercise performance of maximum speed (B), running time (C), running distance (D) of WT ($n = 11$) and *Prmt5^{MKO}* mice ($n = 9$) measured by treadmill.
 E, F Absolute (E) and specific force (F) (on the left panel) and maximal absolute and specific force (on right panel) on EDL muscle from WT ($n = 4$) and *Prmt5^{MKO}* mice ($n = 3$).
 G, H Absolute (G) and specific force (H) (on the left panel) and maximal absolute and specific force (on right panel) on Soleus muscle from WT ($n = 4$) and *Prmt5^{MKO}* mice ($n = 3$). Data information: The data are presented as mean \pm SEM and the P -values by two-tailed ANOVA unpaired t -test based on total number of biologically independent samples indicated in (A–H) (* $P < 0.05$, ** $P < 0.01$, *** $P < 0.001$, **** $P < 0.0001$).

and H). The maximal specific forces of *Prmt5^{MKO}* EDL and Soleus were 27 and 16% lower than the corresponding WT muscles, respectively (Fig 2G and H). These observations indicate that PRMT5 loss-of-function leads to skeletal muscle weakness.

Prmt5 KO reduces oxidative myofibers while increasing glycolytic myofibers

Metabolic properties of myofibers have profound effects on exercise endurance and systemic metabolism (Baskin et al, 2015). We next assessed myofiber composition of representative fast (EDL) and

slow (Soleus) muscles based on immunofluorescent staining of myosin heavy chain isoforms (Fig 3A). A reduced proportion of oxidative type IIA myofibers and an increased proportion of glycolytic type IIB myofibers were observed in EDL and Soleus muscles of *Prmt5^{MKO}* compared with WT muscles (Fig 3B and C). We further carried out succinate dehydrogenase (SDH) staining as an indicator of mitochondrial oxidative capacity (Fig 3D). Compared with the WT EDL muscles, *Prmt5^{MKO}* muscles had a lower abundance of SDH^{high} and SDH^{med} myofibers and a higher abundance of SDH^{low} myofibers (Fig 3E). The *Prmt5^{MKO}* Soleus muscles also had reduced abundance of SDH^{med} myofibers and increased abundance of

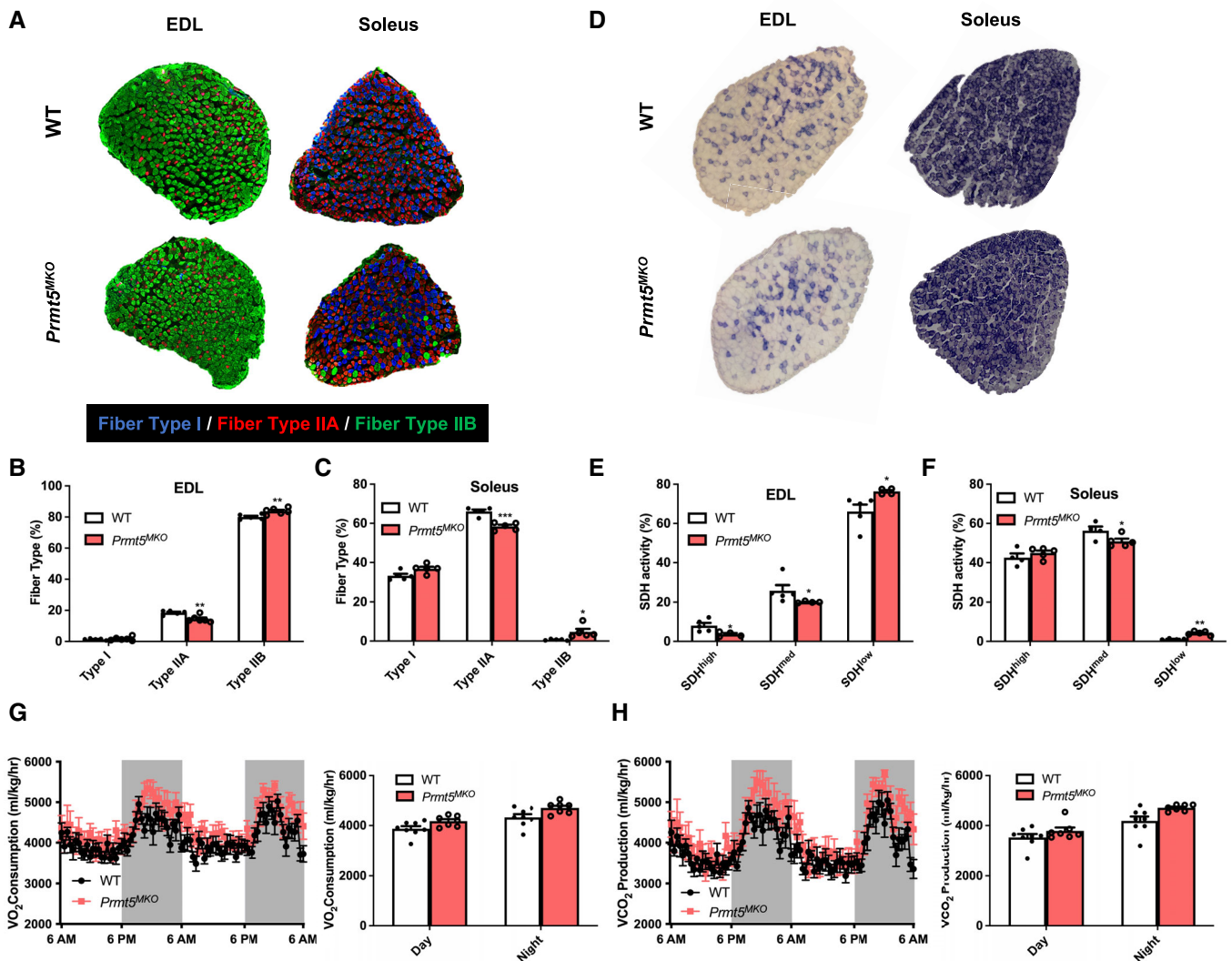


Figure 3. Depletion of *Prmt5* leads to a fiber-type switch toward glycolytic myofibers but does not affect systemic metabolism.

A Representative immunostaining of Type I, IIA, and IIB myofibers in in EDL and Soleus muscles of 2-month-old WT and *Prmt5^{MKO}* mice.
 B, C Quantification of abundance of various fiber types in EDL (B) and Soleus (C) muscles of WT and *Prmt5^{MKO}* mice; ($n = 5$).
 D Representative histochemical staining image of succinate dehydrogenase (SDH) enzymatic activity in EDL and Soleus muscles.
 E, F Quantification of abundance of SDH-low, -medium and -high myofibers in EDL (E) and Soleus (F) muscles of WT ($n = 5$) and *Prmt5^{MKO}* mice ($n = 4$).
 G, H Metabolic rate of O_2 consumption (G) and CO_2 production (H) normalized to lean mass for a 48-h cycle of 4–6-month-old WT ($n = 8$) and *Prmt5^{MKO}* ($n = 7$) mice measured by an indirect calorimetry.

Data information: The data are presented as mean \pm SEM and P -values by two-tailed ANOVA unpaired t -test based on total number of biologically independent samples indicated in (B, C), and (E–H) (* $P < 0.05$, ** $P < 0.01$, *** $P < 0.001$).

SDH^{low} myofibers (Fig 3F). To evaluate the consequence of myofiber type alteration on whole-body metabolism, we used indirect calorimetry to measure the oxygen consumption (VO₂) and carbon dioxide production (VCO₂) (Fig 3G and H). *Prmt5*^{MKO} mice showed similar levels of oxygen consumption (VO₂), carbon dioxide production (VCO₂), and decreased heat production than WT counterparts, during both day and night when the values were normalized to lean masses due to the reduced lean masses in the KO mice (see Fig 1E and 3G and H, and EV3A); however, there are significant differences in the VO₂ and VCO₂ between WT and *Prmt5*^{MKO} mice (Fig EV3B and C). Collectively, these findings suggest that *Prmt5*^{MKO} alters muscle metabolism by shifting oxidative myofibers toward glycolytic myofibers.

PRMT5 regulates lipid metabolism in skeletal muscles

Given the fiber type switching in *Prmt5*^{MKO} mice and well-known metabolic differences among fiber types, we further explored lipid metabolism, which is more pronounced in oxidative myofibers (Jocken *et al.*, 2008). As the first step, we assessed neutral lipid content by Oil Red O (ORO) staining in TA muscle sections and observed in WT muscles under brightfield imaging clusters of myofibers with numerous ORO⁺ lipid droplets, presumably representing oxidative myofibers (Fig 4A). However, ORO⁺ lipid droplets were completely absent in the *Prmt5* KO muscles (Fig 4A). We also used more sensitive fluorescent imaging (as ORO emits red fluorescence) and again observed fluorescent puncta representing lipid droplets in selective clusters of WT myofibers (Fig 4B). In contrast, ORO puncta were absent in *Prmt5*^{MKO} muscles, and only weak and nonpuncta ORO fluorescence were detectable (Fig 4B). These data demonstrate that *Prmt5* KO deregulates lipid metabolism in myofibers.

We further examined the levels of several key proteins involved in lipid metabolism (ATGL/*Pnpla2*, mSREBP1, CEBP-β, FABP4) and downstream mitochondrial electron transport chain (ETC) mediating FAO (Fig 4C). Quantification results showed that the levels of ATGL, a rate-limiting enzyme of lipolysis, were consistently higher but the lipogenic and mitochondrial ETC proteins were all lower in *Prmt5*^{MKO} compared with WT muscles (Fig 4D). We investigated how PRMT5-dependent lipid metabolism affects mitochondrial respiration through Seahorse Analysis in 3-day differentiated myotubes (Fig 4E). The results showed that KO myotubes led to significantly lower levels of oxygen consumption associated with maximal respiration (Max R) and spare capacity (SC) (Fig 4F). The metabolic alterations were not due to differentiation defects because myotube morphology and fusion index (quantified by the number of MyoG⁺ cells ≥ 2 within myotube) remained similar between WT and KO myotubes (Appendix Fig S2). Overall, these findings demonstrate that PRMT5 is crucial for maintaining normal lipid metabolism and mitochondrial respiratory activity in the skeletal muscles.

PRMT5 methylates mSREBP1a to increase its stability

To understand how PRMT5 regulates lipid metabolism in myofibers, we focused on mSREBP1a, a key transcriptional factor regulating lipogenesis that has been reported to be methylated by PRMT5 (Liu *et al.*, 2016). As *Prmt5* KO reduced the level of mSREBP1 (Fig 4C and D), we hypothesized that PRMT5 stabilizes mSREBP1a. We expressed PRMT5-GFP and SREBP1a-Flag fusion proteins in C2C12

myoblasts and confirmed the overexpression of corresponding proteins (Fig 5A). We then performed co-immunoprecipitation (co-IP) using Flag antibody and observed that PRMT5 not only binds to mSREBP1a, but also methylates mSREBP1a (Fig 5A). Conversely, co-IP using GFP antibody (for PRMT5-GFP) also confirmed pull-down of mSREBP1-Flag (Fig 5B). We also performed co-IP and western blots (WB) on WT and *Prmt5*^{MKO} muscles lysates, showing reduced levels of total mSREBP1 and symmetrically dimethylated mSREBP1 in the KO samples (Fig 5C). Notably, the ratio of symmetrically dimethylated mSREBP1 to total mSREBP1 was significantly lower in the *Prmt5*^{MKO} than in the WT muscles (Fig 5D). Consistently, pharmacological inhibition of PRMT5 using BLL3.3 also decreased the dimethylation of mSREBP1a in C2C12 myoblasts (Fig EV4A). These results together demonstrate that PRMT5 mediates dimethylation of mSREBP1.

To explore the biological significance of PRMT5-mediated dimethylation of mSREBP1a, we performed protein stability assay. We overexpressed mSREBP1a with or without PRMT5 in C2C12 myoblasts (Fig 5E). Cells were then treated with cycloheximide (CHX) to inhibit new protein synthesis. Proteins were collected at 0, 4, 8 h after addition of CHX to determine their degradation (Fig 5E). Analysis of mSREBP1a levels over time indicates that PRMT5 expression significantly increased the stability of SREBP1a (Fig 5F). Consistently, *Prmt5*^{MKO} diminished the protein contents of SREBP1 in myotubes differentiated from the mutant myoblasts (Fig EV4B). We also analyzed the expression of SREBP1 target genes responsible for TAG synthesis and fatty acid transport (*Dgat1*, *Dgat2*, and *Fabp4*) in the C2C12 cells overexpressing mSREBP1a alone or together with PRMT5 (Figs 5G and EV4C and D). The results show that PRMT5/SREBP1a co-expression significantly elevated the levels of *Dgat1*, *Dgat2*, and *Fabp4* compared with SREBP1a overexpression-alone group (Fig 5G). This observation demonstrates that dimethylation stabilizes mSREBP1a and increases its transcriptional activity in the presence of PRMT5.

PRMT5 mediates repressive H4R3 dimethylation to regulate *Pnpla2* expression

We next explored how PRMT5 regulates ATGL (encoded by *Pnpla2* gene) expression and lipolysis in muscle cells. PRMT5 has been reported to symmetrically dimethylates arginine residues in histones to repress gene transcription (Ancelin *et al.*, 2006; Wang *et al.*, 2008; Deng *et al.*, 2017). We found that symmetric dimethylation of H4R3 (H4R3Me2s) was significantly reduced in *Prmt5*^{MKO} muscle tissues (Fig 6A and B). In addition, *Pnpla2* expression was upregulated in *Prmt5*^{MKO} muscle tissues but downregulated in PRMT5-overexpressing C2C12 myoblasts (Fig 6C and D). These data prompted us to hypothesize that PRMT5 directly regulates transcription of *Pnpla2* through repressive H4R3Me2s. To test this, we analyzed a ChIP-seq dataset (Jia *et al.*, 2020) and identified a PRMT5 binding peak at around 3,000 bp upstream of transcription start site (TSS) of the *Pnpla2* gene (Fig 6E). ChIP-qPCR analysis confirmed that this region is highly enriched by both PRMT5 and H4R3Me2s in newly differentiated C2C12 myotubes (Fig 6F and G). To substantiate this finding, another ChIP-qPCR assay was performed using WT and *Prmt5*^{MKO} muscle tissues, and *Prmt5*^{MKO} diminished the binding of PRMT5 and H4R3Me2s at the *Pnpla2* promoter region (Fig 6H and I). Taken together, these results

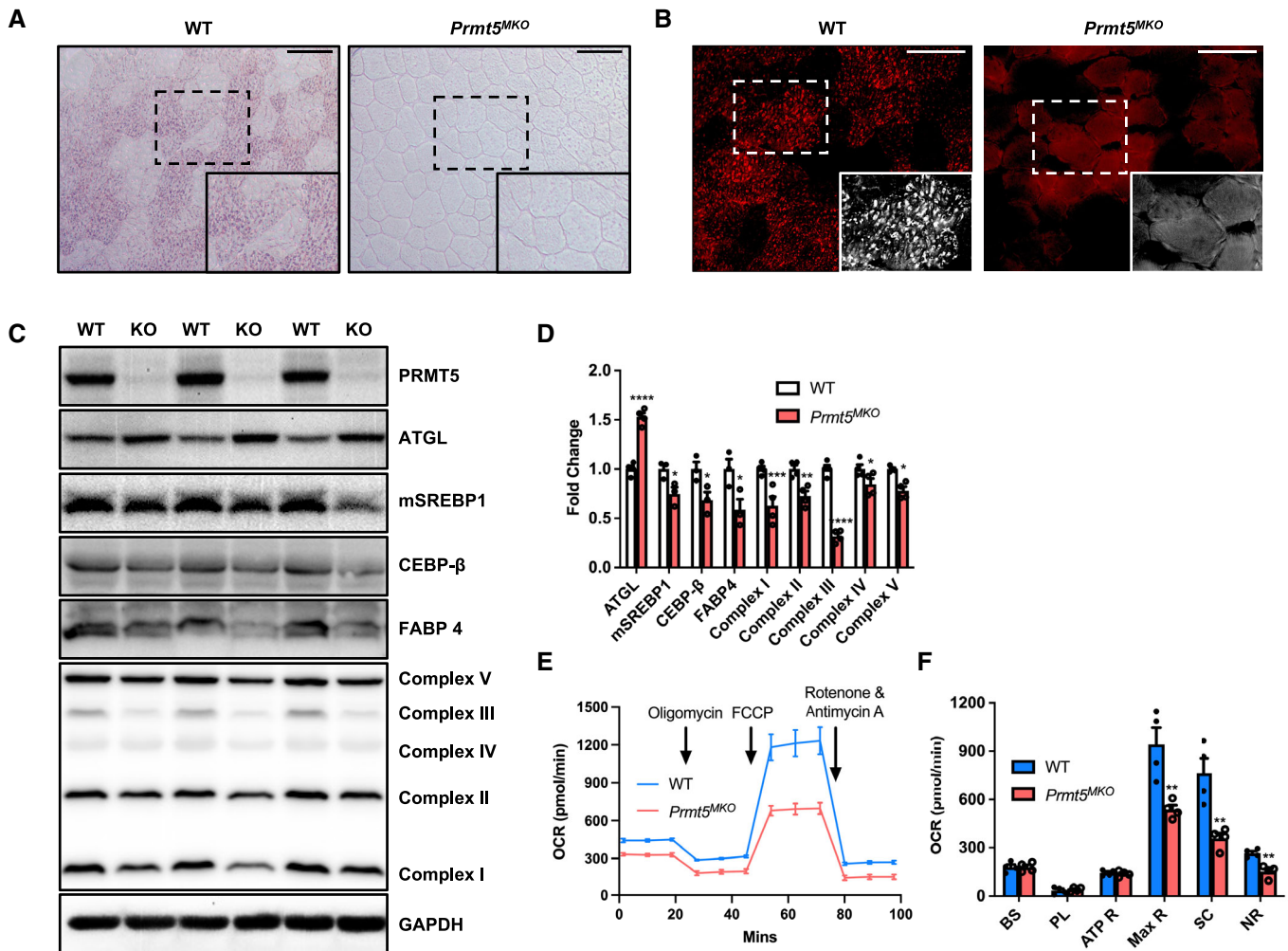


Figure 4. PRMT5-deficient skeletal muscles exhibit lower lipid content and metabolic rate.

A, B Representative images of ORO staining (A) and immunofluorescence (B) in TA muscle from WT and *Prmt5*^{MKO} mice. Scale bar: 100 μm.

C Western blotting analysis for protein markers of lipolysis, lipogenesis, and electron transport chain (ETC) complexes in skeletal muscles of WT (*n* = 3) and *Prmt5*^{MKO} mice; (*n* = 3).

D Quantification of relative protein levels of ATGL, mSREBP1, CEBP-β, FABP4, OXPHOS complexes (normalized to GAPDH) in skeletal muscles of WT and *Prmt5*^{MKO} mice; (*n* = 3).

E Seahorse analysis of oxygen consumption rate (OCR) in myotubes differentiated for 3-days from myoblasts of 4-week-old WT and *Prmt5*^{MKO} mice; (*n* = 4).

F OCR was measured at basal state and after sequential addition of Oligomycin, FCCP, and Rotenone/Antimycin A to determine basal respiration (BS), proton leak (PL), ATP respiration (ATP R), maximal respiration (Max R), spare capacity (SC), and non-mitochondrial respiration (NR); (*n* = 4, technical replicates).

Data information: The data are presented as mean ± SEM and *P*-values by two-tailed ANOVA unpaired *t*-test based on number of biologically independent samples indicated in (D–F) (**P* < 0.05, ***P* < 0.01, ****P* < 0.001, *****P* < 0.0001).

demonstrate that *Pnpla2* is epigenetically repressed by PRMT5 through H4R3Me2s.

Pnpla2 KO normalizes muscle mass and function of the *Prmt5*^{MKO} mice

Adipose triglyceride lipase upregulation drives muscle wasting in cancer cachexia (Das et al, 2011). To directly test whether upregulation of ATGL is responsible for the phenotypes of the *Prmt5*^{MKO} mice, we used *Myl1*^{Cre} to drive muscle-specific double KO of *Prmt5* and *Pnpla2* (*Prmt5/Pnpla2*^{MKO}). Strikingly, the *Prmt5/Pnpla2*^{MKO} mice appeared similar to WT mice, and larger than the *Prmt5*^{MKO} mice (Fig 7A). The body weights and lean masses of the *Prmt5/Pnpla2*^{MKO}

mice were also comparable to those of the WT mice, and higher than those of the *Prmt5*^{MKO} mice (Fig 7B and C). Western blotting confirmed the loss of PRMT5 and ATGL in *Prmt5/Pnpla2*^{MKO} muscles, and the loss of *Prmt5/Pnpla2* restored the levels of mitochondrial ETC proteins in *Prmt5* KO tissue (Fig 7D). The myofiber size was also restored to the WT level in the *Prmt5/Pnpla2*^{MKO} mice (Fig EV5A–C). Performance on the incremental treadmill test and limb grip strength in *Prmt5/Pnpla2*^{MKO} mice were also restored to the WT level (Fig 7E and F). In addition, the alterations in fiber type composition observed in the Soleus and EDL muscles of the *Prmt5*^{MKO} mice were largely normalized in the *Prmt5/Pnpla2*^{MKO} mice (Fig EV5D–F). Moreover, the absolute and specific forces of the EDL and Soleus muscles of *Prmt5/Pnpla2*^{MKO} were significantly higher than that of

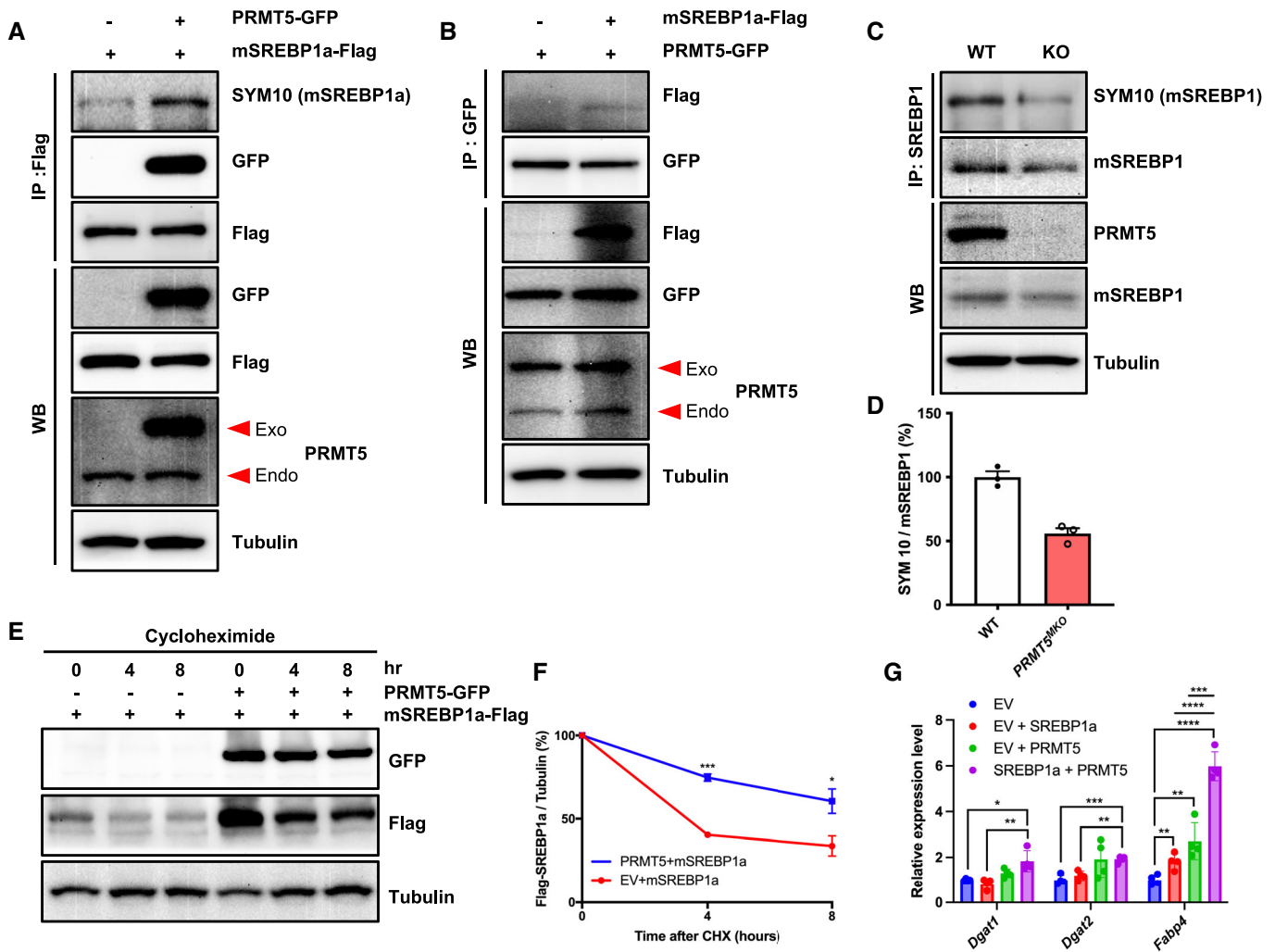


Figure 5. PRMT5 regulates lipid accumulation through SREBP1a methylation and stabilization.

A C2C12 cells overexpressing PRMT5-GFP alone or PRMT5-GFP + SREBP1a-Flag were immunoprecipitated with Flag antibody and blotted with SYM10, GFP, Flag, PRMT5, and Tubulin antibodies. Exo, exogenous (overexpressed); Endo, endogenous.

B C2C12 cells overexpressing SREBP1a-Flag alone or SREBP1a-Flag + PRMT5-GFP were immunoprecipitated with GFP antibody and blotted with Flag, GFP, PRMT5, and Tubulin antibodies.

C Protein extracts of skeletal muscle isolated from WT and *Prmt5*^{MKO} mice were immunoprecipitated with SREBP1 antibody and immunoblotted with SYM10 (mSREBP1), SREBP1, PRMT5, and tubulin antibodies.

D Quantification of methylated mSREBP1 (normalized to total mSREBP1) in (C); ($n = 3$, biological replicates).

E HEK293 cells were transfected with PRMT5-GFP alone or PRMT5-GFP + SREBP1a-Flag for 24 h, followed by cycloheximide (30 $\mu\text{g}/\text{ml}$) and protein analysis at 0, 4, 8 h. Lysates were immunoblotted with Flag, GFP, and tubulin antibodies.

F Intensity of Flag was normalized to tubulin, then normalized to 0 h; ($n = 3$, biological replicates).

G Relative expression of lipogenesis genes (*Dgat1*, *Dgat2*, *Fabp4*) in C2C12 transfected with PRMT5 and SREBP1a; ($n = 4$, technical replicates).

Data information: Data are presented as mean \pm SEM and P -values determined by two-tailed ANOVA unpaired t -test based on total number of biologically independent samples indicated in (D, F, G) (* $P < 0.05$, ** $P < 0.01$, *** $P < 0.001$, **** $P < 0.0001$).

the *Prmt5*^{MKO} mice, with the maximal force of *Prmt5/Prnplal2*^{MKO} mice muscles being identical to that of WT mice (Fig 7C and H, and EV5G and H). We also assessed lipid content by ORO staining in myofibers and found a clear increase in the number of ORO⁺ LDs in *Prmt5/Prnplal2*^{MKO} muscles compared to *Prmt5*^{MKO} muscles under brightfield and fluorescent imaging (Fig 7I). Collectively, these data demonstrate that PRMT5 regulates neutral lipid content, myofiber size, and function through ATGL.

Discussion

Our study uncovers a new role of PRMT5 in myofiber metabolism and contractile function. Utilizing a muscle-specific *Prmt5* KO mouse model, we provided physiological, histological, and molecular evidence to support that PRMT5 ablation leads to muscle atrophy and favors the formation of glycolytic myofibers. Mechanistically, PRMT5 on one hand mediates mSREBP1a methylation to stabilize

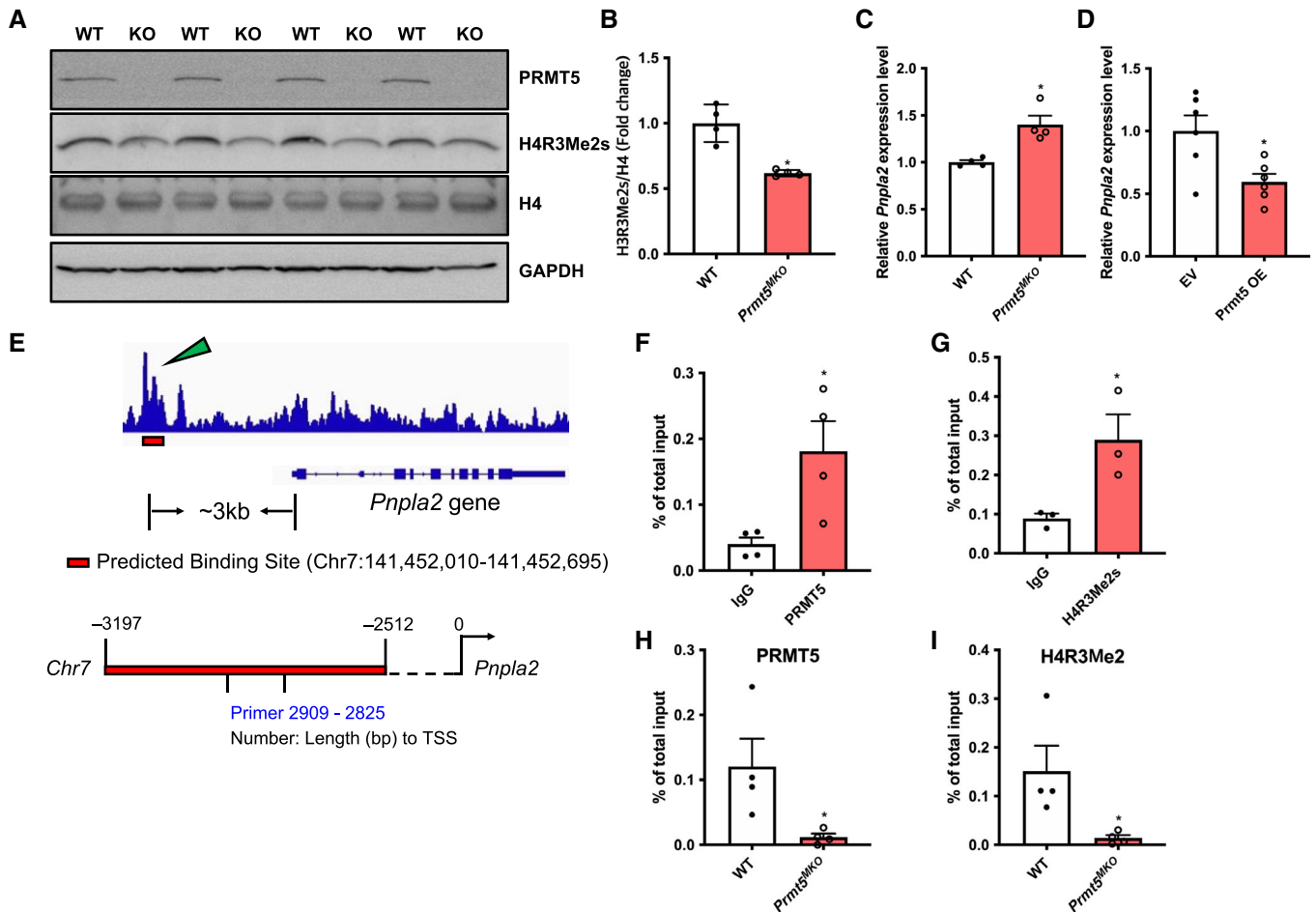


Figure 6. Epigenetic repression of *Pnpla2* transcription by PRMT5 in skeletal muscle.

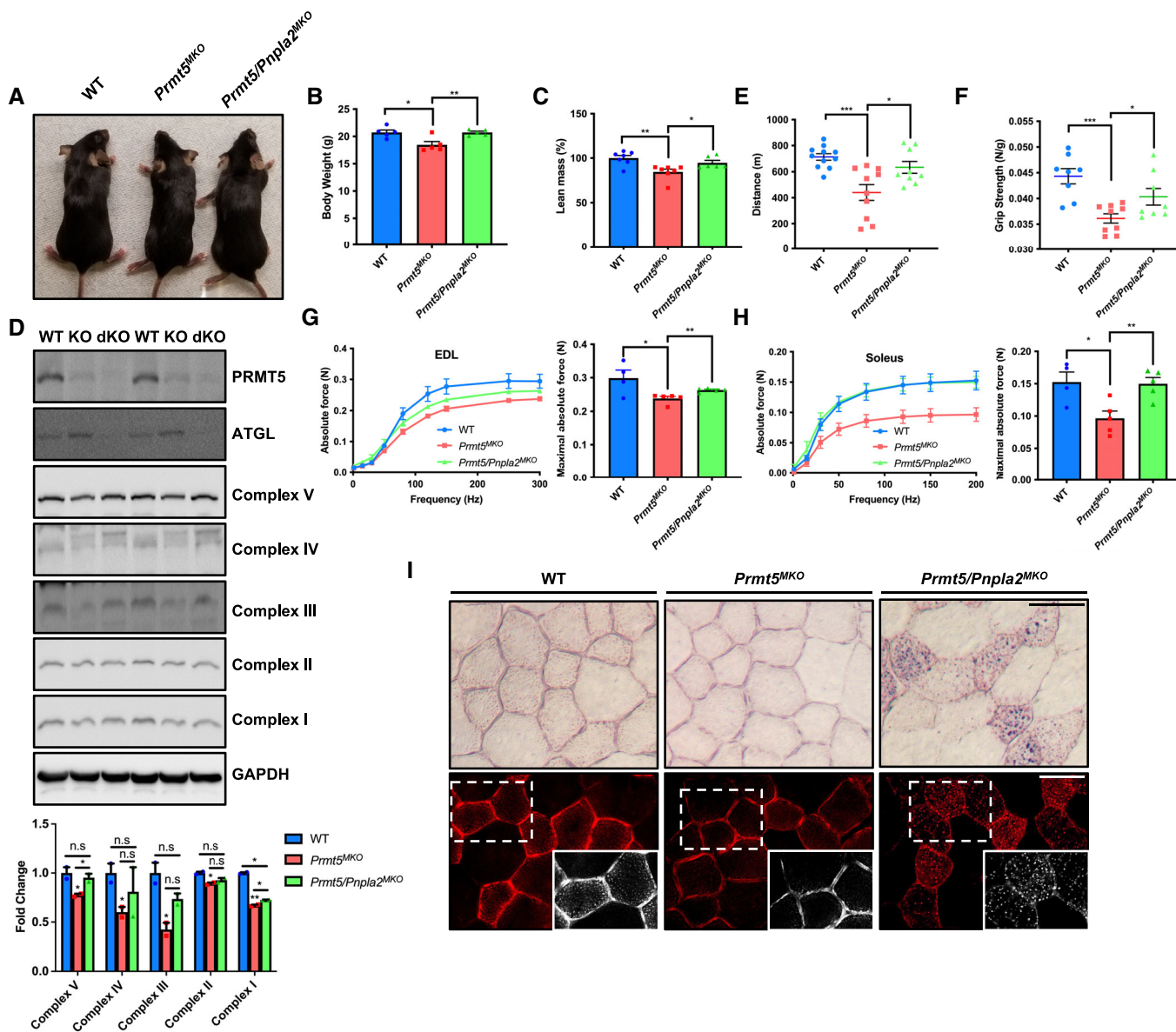
A, B Immunoblots showing symmetric demethylation of H4R3 in skeletal muscles of WT ($n = 4$) and *Prmt5*^{MKO} mice ($n = 4$) (A), and quantification of H4R3Me2s normalized to total H4 (B).
 C Relative *Pnpla2* levels in skeletal muscles of WT and *Prmt5*^{MKO} mice; ($n = 4$)
 D Relative *Pnpla2* levels in *Prmt5*-overexpressed C2C12 myoblasts; ($n = 6$).
 E ChIP-seencing results showing the *Prmt5* binding peak on the *Pnpla2* promoter of 3T3-L1 cells.
 F, G Enrichment of PRMT5 (F) and H4R3Me2s (G) on the proximal promoter region of the *Pnpla2* gene in myotubes; ($n = 4$ for F, $n = 3$ for G, biological replicates).
 H, I Enrichment of PRMT5 (H) and H4R3Me2s (I) on the proximal promoter region of the *Pnpla2* gene in skeletal muscles of WT and *Prmt5*^{MKO} mice ($n = 4$ for H, and I, biological replicates).

Data information: The data are presented as mean \pm SEM and P -values by two-tailed ANOVA unpaired t -test based on total number of biologically independent samples indicated in (B–D), and (F–I) ($*P < 0.05$).

this protein and promote lipogenesis, on the other hand mediates H4R3me2 to repress *Pnpla2* expression and limit lipolysis in myofibers. Thus, PRMT5 should normally promote IMCL deposition through stimulating lipogenesis and limiting lipolysis. Subsequently, concomitant deletion of *Pnpla2* restored muscle functions of the *Prmt5*^{MKO} mice (Fig 8). These results establish a new role of PRMT5 in linking the contractile and metabolic function of myofibers.

Previous work has reported a key role of PRMT5 in regulating proliferation of muscle progenitor cells, and the deletion of *Prmt5* impairs progenitor cell-mediated muscle regeneration (Zhang et al, 2015). *In vitro* studies on PRMT5 have revealed its role in regulating COPR5-mediated cell proliferation and BRG1/MyoD-

dependent chromatin remodeling for myogenic activation within myoblasts (Dacwag et al, 2007; Paul et al, 2012). Although PRMT5 level has been reported to be influenced by exercise in rodent and human skeletal muscles (Vanlieshout et al, 2018, 2019), the specific role of PRMT5 in myofibers has been unknown. This represents a critical knowledge gap given the elevated *Prmt5* expression during myogenic differentiation (Fig EV1). In this work, we used muscle-specific *Myf1*^{Cre} mice to drive the deletion of *Prmt5* in postdifferentiation myofibers. *Myf1* gene is activated at E9 during embryonic development within most skeletal muscles *in vivo* and is expressed in mononuclear myofibers during differentiation *in vitro* (Kelly et al, 1997; Bi et al, 2016). Therefore, the muscle atrophy of the *Prmt5*^{MKO} mice is independent of myogenic differentiation.



In our study, we observed the muscle atrophy of *Prmt5*^{MKO} mice is associated with elevated levels of ATGL, which promotes lipolysis of lipid droplets in myofibers. PRMT5-dependent mSREBP1a methylation in nucleus is reported to upregulate *de novo* lipogenesis in

adipocytes and cancer cells (Liu *et al.*, 2016, 2021; Zhang *et al.*, 2018; Jia *et al.*, 2020; Webb *et al.*, 2020). Our study clearly demonstrated that mSREBP1a is stabilized through methylation by PRMT5, and co-overexpression of *Prmt5* and *Srebp1a* upregulates lipogenic

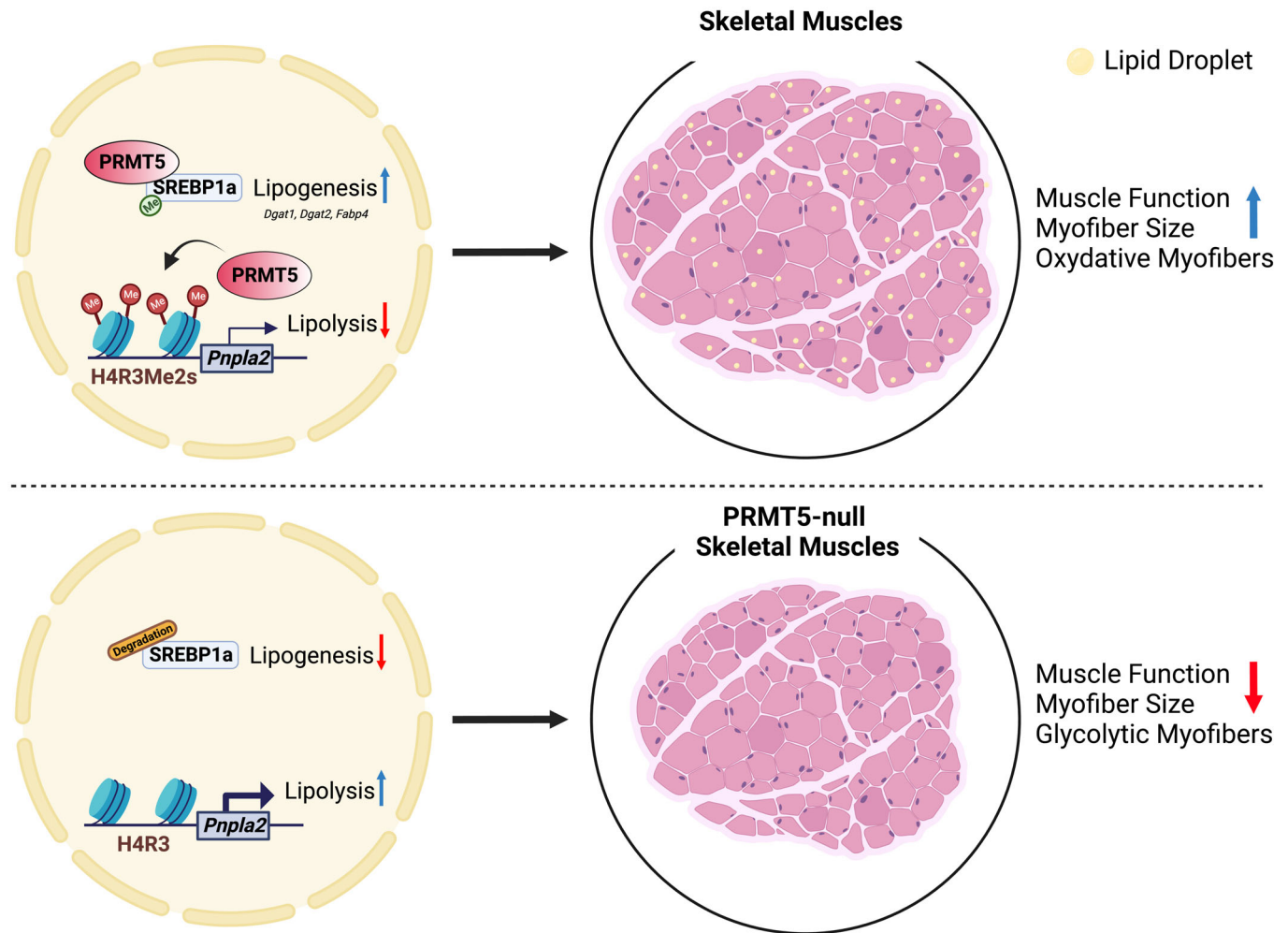


Figure 8. Schematic model depicting the role of PRMT5 in the skeletal muscle.

PRMT5 is highly expressed in skeletal muscle and necessary to mediate symmetric dimethylation of repressive H4R3 at the *Pnpla2* gene, therefore inhibiting lipolysis. PRMT5 also methylates and stabilizes mSREBP1a to promote LD biogenesis. Genetic knockout of *Prmt5* attenuates physical activity and decreases myofiber size accompanied by reduced LD deposition. The deletion of *Pnpla2* *in vivo* can restore the decreased muscle function due to *Prmt5* loss.

genes. Our results suggest that a normal lipid droplet content is necessary for proper function of the muscle. Lipid accumulation in myofibers has been associated with functional declines of muscle in lipid storage myopathies (Vasiljevski *et al*, 2018). Our results demonstrate that a lack of lipids in the myofibers severely compromises muscle contractile function and reduces muscle mass. Our study further suggests that targeting PRMT5 using commercially available pharmacological inhibitors could be a potential therapy for patients with lipid myopathies.

Muscle fiber type switching occurs in response to a variety of genetic, physiological, and metabolic condition (Schiaffino & Reggiani, 2011). A decrease in the proportion of slow-oxidative myofibers is, in general, correlated with reduced exercise plasticity (Park *et al*, 2021). Several PRMTs have been reported to affect fiber type composition (Stouth *et al*, 2018). An increase in the proportion of glycolytic fibers was reported in *Prmt7* KO mice, resulting in reduced endurance exercise capacities (Jeong *et al*, 2016). In our study, loss of PRMT5 protein also converted oxidative myofibers to

glycolytic fiber type, suggesting that PRMT5 is essential for specification or maintenance of the oxidative myofiber types and exercise endurance. Oxidative myofibers normally have a higher mitochondrial content than glycolytic myofibers to enable cellular energy production through oxidative phosphorylation (Hawley, 2002). In pharmacological and genetic inactivation studies *in vivo*, mitochondrial enzyme activity has been shown to be positively associated with exercise capacity (Marcinko *et al*, 2015; Park *et al*, 2021). Consistently, the reduction in oxidative phosphorylation in skeletal muscle tissues and reduced OCR in myofibers of *Prmt5^{MKO}* mice are associated with reduced exercise performance. Glycolytic myofibers normally have higher rate of ATP hydrolysis and generate larger contractile force than slow-twitching oxidative myofibers (Schiaffino & Reggiani, 2011), but the glycolytic fiber type switching in our *Prmt5^{MKO}* mice did not improve muscle force production. This can be explained by the atrophy of these *Prmt5*-null glycolytic myofibers, manifested by significantly reduced myofiber diameter compared with WT glycolytic myofibers. In addition, the mutant

glycolytic myofibers are devoid of LDs, which would reduce muscle energy supply to support contraction. These metabolic alterations may have together accounted for the impaired exercise capacity, as *Pnpla2* KO in *Prmt5*^{MKO} mice rescues not only the lipid droplet content but also muscle contractile functions.

Gene expression and transcription initiation are regulated by numerous epigenetic markers (Ng *et al*, 2009; Moore *et al*, 2013). An epigenetic role of PRMT5 has been shown to regulate chromatin remodeling through histone modification during myogenesis (Tao *et al*, 2011; Paul *et al*, 2012; Gan *et al*, 2019). We show that in terminally differentiated myofibers, PRMT5-mediated H4R3Me2s represents a significant epigenetic regulatory mechanism underlying muscle function and metabolism. We reveal that PRMT5 represses *Pnpla2* expression through directly binding to its promoter. Consistent with our results, PRMT7 and PRMT5 mediate H4R3Me2 represses expression of *Dnmt3b* and *Flip1L*, respectively (Fan *et al*, 2014; Cai *et al*, 2020). Interestingly, SIRT7-mediated desuccinylation at K387 enhances methyltransferase activity of PRMT5 by promoting formation of PRMT5-MEP5 complex to regulate lipid metabolism, and PRMT5 facilitates fatty acid biogenesis through mSREBP1a methylation and BSCL2-mediated lipid droplet formation through methylating SPT5 in adipocytes (Jia *et al*, 2020; Yuan *et al*, 2022). However, the protein levels of ATGL are positively regulated by PRMT5 in adipose tissue but negatively regulated by PRMT5 in myofibers, suggesting tissue-dependent roles of PRMT5 (Jia *et al*, 2020).

Although we show that PRMT5 represses lipolysis in myofibers, whether it also regulates mitochondrial fatty acid oxidation (FAO) remains unknown. Lipid dynamics are modulated by mitochondrial activity, and oxidation of FAs is linked to ATP production for proper muscle function (Eaton, 2002). Patients with lipid storage disorder show disrupted mitochondrial activity in respiratory complexes, and it leads to muscle wasting (Debashree *et al*, 2018; Ji & Yeo, 2019). Furthermore, mitochondrial-targeted antioxidants improved muscle atrophy by preventing reactive oxygen (ROS) production (Min *et al*, 2011). Future studies will be needed to address the involvement of PRMT5 in regulating mitochondrial activity in myofibers.

Materials and Methods

Mice

All procedures involving mice were performed in compliance with the institutional guidelines of Purdue University Animal Care and Use Committee. *Myl1*^{Cre} (Stock # 024713) mouse strains were provided by Steven Burden (Scribal Institute of Biomolecular Medicine, NYU), *Rosa26-Cre*^{ER} (Stock # 008463) mouse strains were bought from Jackson Laboratory, and *Prmt5*^{flox/flox} (Stock # 034414) and *Pnpla2*^{flox/flox} (Stock # 024278) mouse strains were obtained as described previously (Jia *et al*, 2020; Yue *et al*, 2022). The genotypes of experimental WT and KO animals are as follows: WT (*Prmt5*^{flox/flox}), *Prmt5*^{MKO} (*Myl1*^{Cre}, *Prmt5*^{flox/flox}), and *Prmt5/Pnpla2*^{MKO} (*Myl1*^{Cre}, *Prmt5*^{flox/flox}, *Pnpla2*^{flox/flox}). The *Prmt5*^{flox/flox} mice are phenotypically indistinguishable from the *Myl1*^{Cre} and syngeneic wildtype mice. The primers for genotyping are listed in Table EV1. Mice were housed in the animal facility with free access to water and standard rodent chow food or high fat diet (HFD, TD.06414 Harlan). Two-month-old mice were used unless otherwise indicated. Food intake was calculated by

measuring weekly food consumption normalized to body weight in each cage.

Indirect calorimetry study

Oxygen consumption (VO₂) and carbon dioxide production (VCO₂) levels were assessed by using an indirect calorimetry system (Oxymas, Columbus instruments), as previously described (Nie *et al*, 2015). Mice were individually housed in chambers and had free access to food and water under a constant environmental room temperature.

Isolation and culture of primary myoblasts

Primary myoblasts were isolated from hind limb skeletal muscles of 4-week-old mice as previously described (Kim *et al*, 2020). Muscle tissues were minced and digested in type II collagenase and dispase B mixture (Roche). Digestion was neutralized by adding growth media containing F-10 Ham's medium (ThermoFisher Scientific), 20% fetal bovine serum (FBS), 1% penicillin, 4 ng/ml basic fibroblast growth factor (ThermoFisher Scientific), and cells were cultured on collagen-coated plates. Preplating was performed to purify primary myoblasts. For differentiation, primary myoblasts were plated on the BD Matrigel-coated culture plates and differentiated in DMEM supplemented with 2% horse serum and 1% penicillin.

Single myofiber isolation

Single myofibers were isolated from EDL muscles of WT and *Prmt5*^{MKO} mice. Briefly, EDL muscles were carefully dissected and incubated in digestion medium containing 1.5 mg/ml collagenase I in Dulbecco's Modified Eagle's Medium (DMEM, Sigma) at 37°C at the indicated mins (WT for 50 min and *Prmt5*^{MKO} mice for 80 min). EDL muscles were carefully transferred to a preheated plate with 5 ml of DMEM, and single myofibers were released by gently flushing the muscles with a large pore glass pipette. Freshly isolated myofibers were collected for immunofluorescent staining.

Cell cultures and transfection

C2C12 cells were cultured in Dulbecco's modified Eagle's medium (DMEM) supplemented with 10% FBS (Hyclone) and 1% penicillin, in a 37°C humidified incubator with 5% CO₂. For differentiation, C2C12 cells were plated on the BD Matrigel-coated culture plates and differentiated in DMEM supplemented with 2% horse serum, 400 nM insulin, and 1% penicillin. Plasmids and lipofectamine 2000 mixture were transfected in C2C12, based on the manufacturer's instructions, and harvested after 24 h. For transfection, pcDNA-GFP-PRMT5 plasmid and pcDNA3.1-2xFLAG-SREBP1a plasmid were mixed with lipofectamine 2000 Reagent in Opti-MEM media (Gibco) and transfected into 60% confluent cells following the protocol from manufacturer. Opti-MEM media was changed to growth medium after 4 h and cells were harvested after 24 h for further analysis.

scRNA-Seq data analysis

scRNA-seq datasets for muscle satellite cell differentiation were downloaded from publicly available data (GSE150366). For data

analysis, barcodes and reads were aligned to mm10 (*Mus Musculus*) using Cell Ranger v3.1, and data analysis was performed using Seurat v3.1 as previously described (Yue et al, 2022).

H&E, immunofluorescence, and oil red O (ORO) staining

Whole muscle tissues were immediately frozen in optical cutting temperature compound (OCT compound), and subsequently cut into 10- μ m-thick cross sections using a Leica CM1850 cryostat for H&E, immunofluorescence, and Oil red O staining. For H&E staining, the slides were stained in hematoxylin and eosin for 15 and 1 min, respectively, and dehydrated in xylene as previously indicated (Wang et al, 2017). For immunofluorescence staining, cross sections of muscle tissues (TA, EDL, SOL) were fixed in 4% PFA for 15 min and quenched with 100 mM glycine for 10 min. Fixed tissue sections were then incubated with Blocking Buffer (5% goat serum, 2% bovine serum albumin, 0.1% Triton X-100, and 0.1% sodium azide, 1X PBS) for 2 h. Tissue sections were incubated with primary antibodies diluted in blocking buffer overnight at 4°C and incubated with secondary antibodies and DAPI for 1 h at room temperature. For Oil Red O (ORO) staining, muscle tissues were fixed in 4% PFA for 30 min and stained using Oil red O working solutions for 60 min. After washing with running water for 2 min, it was counterstained with hematoxylin, and imaged. All images are representative results of at least four biological replicates. For Succinate dehydrogenase (SDH) staining, muscle tissues were stained with SDH solution (10 ml 0.2 M phosphate buffer, 270 mg sodium succinate, 10 mg NBT) for 10–15 min. The slides were rinsed with deionized H₂O and mount the coverslips with mounting medium.

Muscle injury and regeneration

Muscle injury was induced by CTX injection. After mice were anesthetized by ketamine-xylazine cocktail injection, CTX (50 μ l of 10 μ M solution, Sigma) was injected into TA muscle, and TA muscle was harvested at 5.5-day postinjury to determine regeneration capacity.

Treadmill test and grip strength measurement

Treadmill exercise testing was performed as previously described (Castro & Kuang, 2017). WT, *Prmt5*^{MKO} and *Prmt5/Pnpla2*^{MKO} mice (2 months old), were placed on a treadmill (Eco3/6; Columbus Instruments, Columbus, OH) for 10 min for 3 consecutive days at constant 10 m/min speed for acclimation. On the testing day, mouse ran on the treadmill at 10 m/min for 5 min and the speed was then increased by 2 m/min every 2 min until mice were exhausted. Exercise capacity, including running distance, running time, and maximum speed, was measured. For grip strength, WT, *Prmt5*^{MKO}, and *Prmt5/Pnpla2*^{MKO} mice (2 months old) were tested to measure using a DFE II series Digital Force Gauge (Ametek DFE II 2-LBF 10-N) with an attached metal grid. The mouse was allowed to grasp the metal grid and, and the mouse tail was gently pulled along the axis of the grid. The peak tension at the time of release was recorded. The grip strength was measured three times and the average strength was normalized to body weight (N/g).

Co-immunoprecipitation, protein extraction, and western blot analysis

For Co-IP, C2C12 cells were transfected with pcDNA-GFP-PRMT5 and pcDNA3.1-2xFLAG-SREBP1a, and cells were harvested after 24 h. A total of 500 μ g protein lysate was precleared with protein A/G agarose bead at 4°C for 2 h, and 1 μ g of primary anti-FLAG, or anti-GFP was added into the protein lysate, and rotate for 4 h, followed by addition of protein A/G agarose bead and rotate for overnight.

Total protein was extracted from homogenized muscle tissue using RIPA buffer containing 25 mM Tris-HCl (pH 8.0), 150 mM NaCl, 1 mM EDTA, 0.5% NP-40, and 0.1% SDS, supplemented with proteinase inhibitor and phenylmethylsulphonyl fluoride (PMSF). The concentration of supernatant proteins was quantified using Peirce BCA Protein Assay Reagent (Pierce Biotechnology). Proteins were separated by electrophoresis, transferred to polyvinylidene fluoride (PVDF) membrane, blocked with 5% fat-free milk for 1 h at room temperature and incubated with primary antibodies overnight at 4°C. Antibodies used for western blot analysis were listed in Table EV2. Immunodetection was detected using enhanced chemiluminescence western blotting substrate (Santa Cruz Biotechnology) on a FluorChem R system (Proteinsimple).

Chromatin immunoprecipitation

C2C12 cell-derived myotubes and muscle tissue from both WT and *Prmt5*^{MKO} mice were crosslinked with 1% formaldehyde for 10 min at room temperature and quenched by the addition of 125 mM glycine for 5 min at room temperature. After the samples were washed cold PBS, they were incubated with ChIP cell lysis buffer (20 mM Tris pH 8.0, 0.1%, 85 mM KCl, 0.5% NP40) supplemented with protease inhibitor. After centrifugation, the nuclei were resuspended in nuclei lysis buffer (50 mM Tris pH 8.0, 10 mM EDTA, 1% SDS) and sonicated. The supernatant was used for immunoprecipitation with the indicated antibodies (PRMT5, H4R3Me2s). The immunoprecipitants were eluted and reverse crosslinked overnight at 65°C. Phenol-chloroform method was used to purify DNA fragments and qRT-PCR was performed as indicated. A list of primers used is provided in Table EV1. Results were presented as mean \pm SD from three independent experiments.

Assessment of muscle contractile function

Contractile properties of the slow-twitch soleus and the fast-twitch EDL muscles were measured by using an *in vitro* muscle test system (1200A Intact Muscle Test System, Aurora Scientific). Briefly, the hindlimb was excised under isoflurane anesthesia, and placed in a bicarbonate-buffered solution (137 mM NaCl, 5 mM KCl, 1 mM MgSO₄, 1 mM NaH₂PO₄, 24 mM NaHCO₃, and 2 mM CaCl₂) equilibrated with 95% O₂-5% CO₂. The assessment of contractile function of the EDL muscle was performed first followed by the Soleus muscle. After surgical isolation, braided silk suture thread (4-0, Fine Science Tools) was tied around each end of the muscle tendons. The muscles were then transferred to a tissue bath apparatus containing a bicarbonate-buffered solution at room temperature continuously bubbled with carbogen (95% O₂-5% CO₂) and mounted between two platinum electrodes (1200A Intact Muscle Test System; Aurora Scientific). After the optimal muscle length was determined, the temperature of the glass bath was increased to 32°C, and the

muscles were thermally equilibrated for 10 min. The force–frequency relationship was then generated by selected frequencies between 1 and 300 Hz for the EDL muscle, and 1–200 Hz for Soleus muscle. After completion of the assessment, the muscle was removed from the organ bath, trimmed of connective tissue, blotted dry, and weighed. Muscle cross-sectional area (CSA) was determined by dividing the wet muscle mass by the product of Lo and muscle-specific density (1.056 g/cm³). Specific force (N/cm²) was calculated by dividing the muscle force (N) by the CSA (cm²).

Whole body composition analysis

The Echo-MRI 130 analyzer (EchoMRI LLC, Houston, TX, USA) was used to measure body composition of live mice. After the calibrating the instrument with corn oil, the mouse was gently placed into a cylindrical holder. The holder was inserted into the EcoMRI™ system to measure lean mass, fat mass, and water weight.

Total RNA extraction and qRT-PCR

Total RNA was extracted from cells and tissues using TRIzol reagent (Thermo Fisher Scientific) according to the manufacturer's instruction. A total of 2 µg of total RNA was reversed transcribed with random primers, M-MLV reverse transcriptase and DTT. Real-time qPCR was carried out in a Roche Light cycler 480 PCR system with SYBR green master mix and gene-specific primers, listed in Table EV2. Relative changes in gene expression were analyzed using the 2^{-ΔΔC_T} method and normalized to β-actin.

Seahorse OCR measurement

Primary myoblasts cells (1 × 10⁵ cells) isolated from WT and *Prmt5*^{MKO} mice were seeded in Matrigel coated XF24 microplates (SeaHorse, bioscience). After differentiation for 3 days, myotubes were washed three times with XF medium (supplemented with SeaHorse XF RPMI medium, 5 mM glucose, 2 mM pyruvate, 1 mM glutamine, pH 7.4), and pre-incubated in XF medium for 1 h at 37°C in a non-CO₂ incubator. Oligomycin (3 µM), FCCP (3 µM), Rotenone (1.5 µM), Antimycin A (1.5 µM) were preloaded into cartridges and injected sequentially into XF wells to monitor oxygen consumption rate, OCR (pmol/min). All mitochondria respiration rates were calculated by the SeaHorse Wave software and normalized to the cellular protein contents.

Statistical analysis

All data are presented as mean ± standard error of the mean (SEM). All quantitative analyses were conducted with Student's *t*-test and a two-tail distribution calculated using the GraphPad Prism. Comparisons with *P*-values < 0.05 were considered statistically significant.

Data availability

No new data or codes were generated for this study.

Expanded View for this article is available [online](#).

Acknowledgments

This work was supported by grants from the US National Institutes of Health to S.K. (R01AR078695, R01DK132819, R01AR079235) and S.O. (F31AR077424), and Purdue University Center for Cancer Research (P30CA023168). We also thank Jun Wu, and Mary Larimore for mouse colony maintenance and technical support, and members of the Kuang Laboratory for critical comments.

Author contributions

Kun Ho Kim: Conceptualization; data curation; formal analysis; validation; investigation; visualization; writing – original draft; project administration. **Zhihao Jia:** Conceptualization. **Madigan Snyder:** Formal analysis; investigation. **Jingjuan Chen:** Formal analysis; investigation. **Jiamin Qiu:** Formal analysis; investigation. **Stephanie N Oprescu:** Formal analysis; investigation. **Xiyue Chen:** Formal analysis; investigation. **Sabriya A Syed:** Formal analysis; investigation. **Feng Yue:** Conceptualization. **Bruno T Roseguini:** Formal analysis; methodology. **Anthony N Imbalzano:** Conceptualization; methodology. **Changdeng Hu:** Conceptualization; methodology. **Shihuan Kuang:** Conceptualization; formal analysis; supervision; project administration; writing – review and editing.

Disclosure and competing interests statement

The authors declare that they have no conflict of interest.

References

- Ancelin K, Lange UC, Hajkova P, Schneider R, Bannister AJ, Kouzarides T, Surani MA (2006) Blimp1 associates with Prmt5 and directs histone arginine methylation in mouse germ cells. *Nat Cell Biol* 8: 623–630
- Badin P-M, Loubière C, Coonen M, Louche K, Tavernier G, Bourlier V, Mairal A, Rustan AC, Smith SR, Langin D *et al* (2012) Regulation of skeletal muscle lipolysis and oxidative metabolism by the co-lipase CGI-58. *J Lipid Res* 53: 839–848
- Baskin KK, Winders BR, Olson EN (2015) Muscle as a “mediator” of systemic metabolism. *Cell Metab* 21: 237–248
- Bassel-Duby R, Olson EN (2006) Signaling pathways in skeletal muscle remodeling. *Annu Rev Biochem* 75: 19–37
- Bi P, Yue F, Sato Y, Wirbisky S, Liu W, Shan T, Wen Y, Zhou D, Freeman J, Kuang S (2016) Stage-specific effects of notch activation during skeletal myogenesis. *Elife* 5: e17355
- Bonaldo P, Sandri M (2013) Cellular and molecular mechanisms of muscle atrophy. *Dis Model Mech* 6: 25–39
- Cai S, Wang P, Xie T, Li Z, Li J, Lan R, Ding Y, Lu J, Ye J, Wang J *et al* (2020) Histone H4R3 symmetric di-methylation by Prmt5 protects against cardiac hypertrophy via regulation of Filip1L/β-catenin. *Pharmacol Res* 161: 105104
- Castro B, Kuang S (2017) Evaluation of muscle performance in mice by treadmill exhaustion test and whole-limb grip strength assay. *Bio Protoc* 7: e2237
- Chargé SBP, Rudnicki MA (2004) Cellular and molecular regulation of muscle regeneration. *Physiol Rev* 84: 209–238
- Choi S, Jeong H-J, Kim H, Choi D, Cho S-C, Seong JK, Koo S-H, Kang J-S (2019) Skeletal muscle-specific Prmt1 deletion causes muscle atrophy via deregulation of the PRMT6-FOXO3 axis. *Autophagy* 15: 1069–1081
- Cossitt LA, Bell JA, Houmard JA (2009) Intramuscular lipid metabolism, insulin action, and obesity. *IUBMB Life* 61: 47–55
- Dacwag CS, Ohkawa Y, Pal S, Sif S, Imbalzano AN (2007) The protein arginine methyltransferase Prmt5 is required for myogenesis because it facilitates ATP-dependent chromatin remodeling. *Mol Cell Biol* 27: 384–394

- Das SK, Eder S, Schauer S, Diwoky C, Temmel H, Guertl B, Gorkiewicz G, Tamilarasan KP, Kumari P, Trauner M et al (2011) Adipose triglyceride lipase contributes to cancer-associated cachexia. *Science* 333: 233–238
- Debashree B, Kumar M, Keshava Prasad TS, Natarajan A, Christopher R, Nalini A, Bindu PS, Gayathri N, Srinivas Bharath MM (2018) Mitochondrial dysfunction in human skeletal muscle biopsies of lipid storage disorder. *J Neurochem* 145: 323–341
- Deng X, Shao G, Zhang H-T, Li C, Zhang D, Cheng L, Elzey BD, Pili R, Ratliff TL, Huang J et al (2017) Protein arginine methyltransferase 5 functions as an epigenetic activator of the androgen receptor to promote prostate cancer cell growth. *Oncogene* 36: 1223–1231
- Dubé JJ, Sitnick MT, Schoiswohl G, Wills RC, Basantani MK, Cai L, Puliniakunil T, Kershaw EE (2015) Adipose triglyceride lipase deletion from adipocytes, but not skeletal myocytes, impairs acute exercise performance in mice. *Am J Physiol Endocrinol Metab* 308: E879–E890
- Eaton S (2002) Control of mitochondrial β -oxidation flux. *Prog Lipid Res* 41: 197–239
- Fan H, Zhang Z, Wang N, Cui Y, Sun H, Liu Y, Wu H, Zheng S, Bao S, Ling H (2014) SKB1/PRMT 5-mediated histone H 4 R 3 dimethylation of I b subgroup bHLH genes negatively regulates iron homeostasis in *Arabidopsis thaliana*. *Plant J* 77: 209–221
- Gan YM, Zhou J, Quan R, Hong LJ, Li Z, Zheng EQ, Liu W, Wu ZF, Cai GY, Gu T (2019) Histone H3K27me3 in the regulation of skeletal muscle development. *Yi Chuan* 41: 285–292
- Guccione E, Richard S (2019) The regulation, functions and clinical relevance of arginine methylation. *Nat Rev Mol Cell Biol* 20: 642–657
- Hagen RM, Rodriguez-Cuenca S, Vidal-Puig A (2010) An allostatic control of membrane lipid composition by SREBP1. *FEBS Lett* 584: 2689–2698
- Hawley JA (2002) Adaptations of skeletal muscle to prolonged, intense endurance training. *Clin Exp Pharmacol Physiol* 29: 218–222
- Jeong H-J, Lee H-J, Vuong TA, Choi K-S, Choi D, Koo S-H, Cho SC, Cho H, Kang J-S (2016) Prmt7 deficiency causes reduced skeletal muscle oxidative metabolism and age-related obesity. *Diabetes* 65: 1868–1882
- Jeong H-J, Lee S-J, Lee H-J, Kim H-B, Vuong TA, Cho H, Bae G-U, Kang J-S (2020) Prmt7 promotes myoblast differentiation via methylation of p38MAPK on arginine residue 70. *Cell Death Differ* 27: 573–586
- Ji LL, Yeo D (2019) Mitochondrial dysregulation and muscle disuse atrophy. *F1000Res* 8:
- Jia Z, Yue F, Chen X, Narayanan N, Qiu J, Syed SA, Imbalzano AN, Deng M, Yu P, Hu C et al (2020) Protein arginine methyltransferase PRMT5 regulates fatty acid metabolism and lipid droplet biogenesis in white adipose tissues. *Adv Sci* 7: 2002602
- Jocken JWE, Smit E, Goossens GH, Essers YPG, van Baak MA, Mensink M, Saris WHM, Blaak EE (2008) Adipose triglyceride lipase (ATGL) expression in human skeletal muscle is type I (oxidative) fiber specific. *Histochem Cell Biol* 129: 535–538
- Kelly RG, Zammit PS, Schneider A, Alonso S, Biben C, Buckingham ME (1997) Embryonic and fetal myogenic programs act through separate enhancers at the MLC1F/3F locus. *Dev Biol* 187: 183–199
- Kim G, Kim JH (2020) Impact of skeletal muscle mass on metabolic health. *Endocrinol Metab* 35: 1–6
- Kim J, Wei Y, Sowers JR (2008) Role of mitochondrial dysfunction in insulin resistance. *Circ Res* 102: 401–414
- Kim KH, Qiu J, Kuang S (2020) Isolation, culture, and differentiation of primary myoblasts derived from muscle satellite cells. *Bio Protoc* 10: e3686
- Lee DY, Teyssier C, Strahl BD, Stallcup MR (2005) Role of protein methylation in regulation of transcription. *Endocr Rev* 26: 147–170
- Litt M, Qiu Y, Huang S (2009) Histone arginine methylations: their roles in chromatin dynamics and transcriptional regulation. *Biosci Rep* 29: 131–141
- Liu L, Zhao X, Zhao L, Li J, Yang H, Zhu Z, Liu J, Huang G (2016) Arginine methylation of SREBP1a via PRMT5 promotes de novo lipogenesis and tumor growth. *Cancer Res* 76: 1260–1272
- Liu L, Yan H, Ruan M, Yang H, Wang L, Lei B, Sun X, Chang C, Huang G, Xie W (2021) An AKT/PRMT5/SREBP1 axis in lung adenocarcinoma regulates de novo lipogenesis and tumor growth. *Cancer Sci* 112: 3083–3098
- di Lorenzo A, Bedford MT (2011) Histone arginine methylation. *FEBS Lett* 585: 2024–2031
- Marcinko K, Bujak AL, Lally JS, Ford RJ, Wong TH, Smith BK, Kemp BE, Jenkins Y, Li W, Kinsella TM et al (2015) The AMPK activator R419 improves exercise capacity and skeletal muscle insulin sensitivity in obese mice. *Mol Metab* 4: 643–651
- Meex RC, Hoy AJ, Mason RM, Martin SD, McGee SL, Bruce CR, Watt MJ (2015) ATGL-mediated triglyceride turnover and the regulation of mitochondrial capacity in skeletal muscle. *Am J Physiol Endocrinol Metab* 308: E960–E970
- Min K, Smuder AJ, Kwon O, Kavazis AN, Szeto HH, Powers SK (2011) Mitochondrial-targeted antioxidants protect skeletal muscle against immobilization-induced muscle atrophy. *J Appl Physiol* 111: 1459–1466
- Moore LD, Le T, Fan G (2013) DNA methylation and its basic function. *Neuropsychopharmacology* 38: 23–38
- Morales PE, Bucarey JL, Espinosa A (2017) Muscle lipid metabolism: role of lipid droplets and perilipins. *J Diabetes Res* 2017: 1–10
- Murn J, Shi Y (2017) The winding path of protein methylation research: milestones and new frontiers. *Nat Rev Mol Cell Biol* 18: 517–527
- Ng SS, Yue WW, Oppermann U, Klose RJ (2009) Dynamic protein methylation in chromatin biology. *Cell Mol Life Sci* 66: 407–422
- Nie Y, Gavin TP, Kuang S (2015) Measurement of resting energy metabolism in mice using oxymax open circuit indirect calorimeter. *Bio Protoc* 5: e1602
- Olzmann JA, Carvalho P (2019) Dynamics and functions of lipid droplets. *Nat Rev Mol Cell Biol* 20: 137–155
- Onal G, Kutlu O, Gozuacik D, Dokmeci Emre S (2017) Lipid droplets in health and disease. *Lipids Health Dis* 16: 1–15
- Park B-H, Song M-Y, Han CY, Moon YJ, Bae EJ (2021) Sirt6 reprograms myofibers to oxidative type through CREB-dependent Sox6 suppression. *Nat Commun* 13: 1808
- Paul C, Sardet C, Fabbriozzi E (2012) The histone-and PRMT5-associated protein COPR5 is required for myogenic differentiation. *Cell Death Differ* 19: 900–908
- Sandri M (2008) Signaling in muscle atrophy and hypertrophy. *Phys Ther* 23: 160–170
- Schiaffino S, Reggiani C (2011) Fiber types in mammalian skeletal muscles. *Physiol Rev* 91: 1447–1531
- Seibert JT, Najt CP, Heden TD, Mashek DG, Chow LS (2020) Muscle lipid droplets: cellular signaling to exercise physiology and beyond. *Trends Endocrinol Metab* 31: 928–938
- Sitnick MT, Basantani MK, Cai L, Schoiswohl G, Yazbeck CF, Distefano G, Ritov V, DeLany JP, Schreiber R, Stolz DB et al (2013) Skeletal muscle triacylglycerol hydrolysis does not influence metabolic complications of obesity. *Diabetes* 62: 3350–3361
- Stouth DW, Manta A, Ljubicic V (2018) Protein arginine methyltransferase expression, localization, and activity during disuse-induced skeletal muscle plasticity. *Am J Physiol Cell Physiol* 314: C177–C190
- Tao Y, Nepl RL, Huang Z-P, Chen J, Tang R-H, Cao R, Zhang Y, Jin S-W, Wang D-Z (2011) The histone methyltransferase Set7/9 promotes myoblast differentiation and myofibril assembly. *J Cell Biol* 194: 551–565

- Uhlén M, Fagerberg L, Hallström BM, Lindskog C, Oksvold P, Mardinoglu A, Sivertsson Å, Kampf C, Sjöstedt E, Asplund A et al (2015) Tissue-based map of the human proteome. *Science* 347: 1260419
- VanLieshout TL, Stouth DW, Tajik T, Ljubicic V (2018) Exercise-induced protein arginine methyltransferase expression in skeletal muscle. *Med Sci Sports Exerc* 50: 447–457
- VanLieshout TL, Bonafiglia JT, Gurd BJ, Ljubicic V (2019) Protein arginine methyltransferase biology in humans during acute and chronic skeletal muscle plasticity. *J Appl Physiol* 127: 867–880
- Vasiljevski ER, Summers MA, Little DG, Schindeler A (2018) Lipid storage myopathies: current treatments and future directions. *Prog Lipid Res* 72: 1–17
- Wang Y, Pessin JE (2013) Mechanisms for fiber-type specificity of skeletal muscle atrophy. *Curr Opin Clin Nutr Metab Care* 16: 243–250
- Wang L, Pal S, Sif S (2008) Protein arginine methyltransferase 5 suppresses the transcription of the RB family of tumor suppressors in leukemia and lymphoma cells. *Mol Cell Biol* 28: 6262–6277
- Wang S-CM, Dowhan DH, Eriksson NA, Muscat GEO (2012) CARM1/PRMT4 is necessary for the glycogen gene expression programme in skeletal muscle cells. *Biochem J* 444: 323–331
- Wang C, Yue F, Kuang S (2017) Muscle histology characterization using H&E staining and muscle fiber type classification using immunofluorescence staining. *Bio Protoc* 7: e2279
- Watt MJ, Hoy AJ (2012) Lipid metabolism in skeletal muscle: generation of adaptive and maladaptive intracellular signals for cellular function. *Am J Physiol Endocrinol Metab* 302: E1315–E1328
- Webb LM, Sengupta S, Edell C, Piedra-Quintero ZL, Amici SA, Miranda JN, Bevins M, Kennemer A, Laliotis G, Tsiichlis PN et al (2020) Protein arginine methyltransferase 5 promotes cholesterol biosynthesis-mediated Th17 responses and autoimmunity. *J Clin Invest* 130: 1683–1698
- Welte MA, Gould AP (2017) Lipid droplet functions beyond energy storage. *Biochim Biophys Acta Mol Cell Biol Lipids* 1862: 1260–1272
- Yuan H, Zhao M, Zhao L, Yun H, Yang G, Geng Y, Wang Y, Zheng W, Yuan Y, Song T et al (2022) PRMT5 confers lipid metabolism reprogramming, tumour growth and metastasis depending on the SIRT7-mediated desuccinylation of PRMT5 K387 in tumours. *Acta Pharmacol Sin* 43: 1–13
- Yue F, Oprescu SN, Qiu J, Gu L, Zhang L, Chen J, Narayanan N, Deng M, Kuang S (2022) Lipid droplet dynamics regulate adult muscle stem cell fate. *Cell Rep* 38: 110267
- Zhang T, Günther S, Looso M, Künne C, Krüger M, Kim J, Zhou Y, Braun T (2015) Prmt5 is a regulator of muscle stem cell expansion in adult mice. *Nat Commun* 6: 1–14
- Zhang X, Wu J, Wu C, Chen W, Lin R, Zhou Y, Huang X (2018) The LINC01138 interacts with PRMT5 to promote SREBP1-mediated lipid desaturation and cell growth in clear cell renal cell carcinoma. *Biochem Biophys Res Commun* 507: 337–342



License: This is an open access article under the terms of the [Creative Commons Attribution-NonCommercial-NoDerivs](https://creativecommons.org/licenses/by-nc-nd/4.0/) License, which permits use and distribution in any medium, provided the original work is properly cited, the use is non-commercial and no modifications or adaptations are made.